J Solid State Electrochem (2010) 14:2083–2088
DOI 10.1007/s10008-010-1039-3

ORIGINAL PAPER

# Electrochemical synthesis of ZnO coatings from water–isopropanol mixed baths: control over oriented crystallization

**Belavalli E. Prasad · P. Vishnu Kamath**

Received: 16 November 2009 / Revised: 19 January 2010 / Accepted: 26 February 2010 / Published online: 27 March 2010


**Abstract** Electroreduction of an aqueous solution of a soluble Zn salt results in the deposition of ZnO crystallites with hexagonal columnar morphology. The crystallites grow with their long axes normal to the substrate resulting in adherent coatings with a strong *c*-axis orientation. This phenomenon is on account of the polarity of the 001 crystal face combined with the high dielectric constant of water. When the dielectric constant of the solvent is changed by making a mixture of water and isopropanol, there is a change in the direction of orientation of the coating. The switch takes place in the sequence [001] → [102], [103] → unoriented → [100], [110] as the isopropanol concentration is raised in a step-wise manner to 60% (*v*/*v*). The switch in orientation is caused by the tilt of the long axes of the hexagonal columns of ZnO with respect to the normal to the substrate. Above 60% isopropanol concentration, ZnO deposition is suppressed. This work demonstrates solution-mediated control over oriented crystallization.

**Keywords** Electrodeposition · ZnO · Oriented crystallization · Crystallite morphology

## Introduction

ZnO is a *n*-type semiconductor with wurtzite structure and a band gap of 3.3 eV at ambient temperature [1]. ZnO is of considerable interest in contemporary materials science because of its many useful applications in the emerging field of oxide optoelectronics [2]. In addition, it is used as a phosphor [3], catalyst [4], and a general ceramic [5]. Thin films of ZnO are transparent and conducting [6].

ZnO films and coatings are generally made by radio frequency (rf) sputtering [6], metalorganic chemical vapor deposition (CVD) [7], atomic layer epitaxy [8], CVD [9], and electrodeposition [10–23]. Among all these techniques, electrodeposition is the simplest, as it obviates the need for high-vacuum and high-power laser/rf/ion beam sources. In addition, electrodeposition is an ambient temperature technique.

Izaki and Omi [10–12] reported the electrodeposition of ZnO by cathodic reduction of an aqueous solution of a soluble salt of Zn. They explored empirically the various deposition conditions that yielded oriented, highly conducting micrometer-thick coatings of ZnO on transparent conducting glass substrates. However, it was Lincot and coworkers [14, 18, 19, 21] who, in a series of papers, investigated the kinetics and mechanism of ZnO electrodeposition. They obtained by experiment and theory the conditions required for the nucleation of ZnO in preference to other competing phases such as $Zn(OH)_2$ and the basic salts of Zn. They also used a variety of substrates, such as oriented GaN(0002) [15, 16, 20], Au [14], and spray pyrolyzed $SnO_2$ [17]. A number of precursors for the oxide ion as well as $Zn^{2+}$ ion were explored [16–19]. Two features are common to all these studies:

1. The ZnO coatings are all oriented strongly along the [001] direction.
2. In all cases, the crystallites have a columnar morphology; the cross section of the columns is hexagonal. The strong out-of-plane orientation is the result of the long axis of the columns, also the *c*-crystallographic axis of ZnO, being perpendicular to the substrate.

**Electronic supplementary material** The online version of this article (doi:10.1007/s10008-010-1039-3) contains supplementary material, which is available to authorized users.

B. E. Prasad · P. V. Kamath (✉)
Department of Chemistry, Central College, Bangalore University, Bangalore 560 001, India
e-mail: vishnukamath8@hotmail.com

The results remain unchanged even when single crystalline substrates of GaN [15, 16, 20] or Au [22, 23] were used. Single crystalline substrates facilitate in-plane orientation as well, by virtue of which the hexagonal columns are rotated to minimize the strain due to lattice mismatch [22]. Anodic deposition from an alkaline zincate bath also yielded a strong [001] out-of-plane orientation and columnar morphology. These observations indicate that the [001] oriented crystallization under the potential gradient of the double layer is driven by the factors inherent to the structure of ZnO rather than experimental factors such as bath composition or deposition conditions. Indeed, the (001) plane of ZnO has a low surface energy, as a result of which crystallite growth takes place in-plane rather than along the direction normal to it [23]. This kind of growth is thermodynamics driven. At high deposition currents, when the growth is kinetically driven [12], the orientation is lost, as the hexagonal columns grow with a random tilt of their long axes to the substrate surface.

One of the problems confronting the electrodeposition of ZnO is codeposition of zinc hydroxide or the basic salts of Zn [14]. This can generally be avoided by using a nonaqueous bath such as DMSO, where dissolved $O_2$ reduction can be used to generate the oxide ion. Formation of $Zn(OH)_2$ can be suppressed by carrying out the electrodeposition at an elevated temperature (100 °C) [24]. These films were also textured along the [001] direction.

Since the photoluminescence of ZnO is *k*-dependent [25], there is interest in the growth of ZnO coatings with different orientations. In this study, we use a mixed $H_2O$/isopropanol (IPA) bath and report differently oriented ZnO coatings.

## Experimental

### Synthesis

ZnO coatings were deposited from $Zn(NO_3)_2$ baths (0.04 M) prepared using water–IPA mixed solvent (0–60%, *v*/*v* IPA). $Zn(NO_3)_2$ and IPA were purchased from Merck, India and used as such. All the solutions were prepared using ion-exchanged type-I water (Milli-Q Academic water purification system, specific resistance 18.2 MΩ cm).

Electrodeposition was carried out using an EG&G Versastat IIA scanning potentiostat driven by Powersuite software. A stainless steel flag (SS 304, area 4.5 $cm^2$) was used as cathode, and a cylindrical Pt mesh (geometric area 28 $cm^2$) was used as the counter electrode. Deposition was carried out potentiostatically at −0.9 V with respect to saturated calomel electrode. The deposition time was varied from 60 to 90 min, and deposition temperature was maintained at 60 °C. After deposition, the coatings were cleaned with water and dried at 65 °C. Prior to electrodeposition, stainless steel electrodes were degreased with detergent and electrochemically polished by polarizing them anodically (30 s) and then cathodically (30 s) in 1 M KOH solution and again anodically (30 s) in 1 M HCl (current density 20 mA $cm^{-2}$) [26].

Mass of the coatings was determined by weighing the stainless steel flags before and after deposition. Thickness of the coatings was estimated using the density of ZnO (5,606 kg $m^{-3}$). The mass and thickness of the coatings are given in Table 1. As the observed coatings are porous, the thickness in Table 1 is only an approximate estimate of the average value.

### Characterization

All coatings were characterized by X-ray diffraction (XRD), by mounting the electrode directly onto a Bruker aXS D8 Advance diffractometer (Cu K$\alpha$ source $\lambda$= 1.541 Å). XRD profiles were fit by the Rietveld method (FullProf suite), using the published structure of ZnO (ICSD No.cF56; $P6_3mc$, $a$=3.2494 Å, $c$=5.2054 Å). The quality of the fit was judged from the *R* values and also by an examination of the difference profile. The observation of systematic residual intensities in the difference profile at

**Table 1** Characteristics of ZnO coatings obtained with baths of different compositions

| Bath composition (%, *v*/*v*)[a] | Mass (mg) | Approximate average thickness (μm) | March function parameters | | | |
|---|---|---|---|---|---|---|
| | | | $G_1$ | $G_2$ | Orientation | Fractions |
| 0 | 16.7 | 6.6 | | | 001 | |
| 40 | 17.8 | 7.04 | 0.56 | 0.42 | 102 | 0.49 |
| | | | | | 103 | 0.38 |
| 50 | 19.1 | 7.5 | | | – | |
| 60 | 20.7 | 8.2 | 0.28 | 0.96 | 100 | 0.69 |
| | | | | | 110 | 0.74 |

[a] Percentage of isopropanol

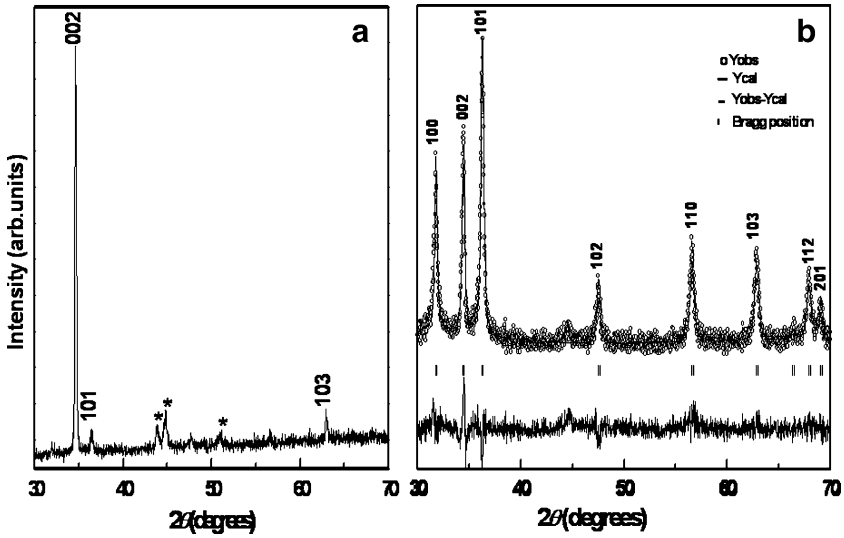


**Fig. 1** XRD profile of a ZnO coating obtained from **a** an aqueous bath and **b** Rietveld refinement of the structure of a powder sample of ZnO obtained by grinding many coatings of the type shown in **a**

positions corresponding to the different Bragg reflections is indicative of oriented crystallization [27]. In such cases, the Rietveld refinement was repeated by the inclusion of the modified March function to account for the orientation. The March function has two refinable parameters, $G_1$ and $G_2$. Of importance in the present context is $G_2$. $G_2$=0 corresponds to a fully oriented coating, while $G_2$=1 to a coating without any preferred orientation. Reflections due to the substrate were excluded in the refinement process. Surface morphologies were studied using a scanning electron microscope (JEOL Model JSM 6490LV microscope, operating voltage 15 kV) by mounting the as-prepared coatings on conducting carbon tape and sputter coating with Pt to improve the conductivity.

## Results and discussion

The XRD pattern of a ZnO coating obtained from an aqueous bath (Fig. 1a) has only one prominent peak at 34.4° 2$\theta$ ($d$=2.603 Å) corresponding to the (002) plane of ZnO. Two minor peaks appear at 2$\theta$ values corresponding to the (101) and (103) planes. To facilitate phase identification, many such coatings were ground together. The XRD pattern of this polycrystalline powder sample exhibits all the reflections expected of wurtzite ZnO, and a Rietveld fit of the profile (Fig. 1b) yields the structure of ZnO (space group $P6_3mc$, refined parameters $a$=3.2506(2) Å, $c$=5.2079 (5) Å). We conclude that Fig. 1a corresponds to a coating of ZnO with a strong $c$-axis orientation. These results are in keeping with numerous previous reports.

The nature of the coating remained unchanged at low (10–30%, $v/v$) IPA concentrations. When the IPA content was raised to 35–40% ($v/v$), a dramatic change in the XRD pattern was observed. Although the pattern exhibits all the reflections expected of ZnO, the intensity of the reflection due to the (103) plane at 62.9° 2$\theta$ ($d$=1.477 Å) is enhanced greatly relative to that of the (110) plane (see Supporting Information SI 1; Fig. 2a). The reflection due to the (002) plane is progressively attenuated (compare Fig. 1a with SI 1). On performing a Rietveld fit of the profile shown in Fig. 2a, residual intensities were seen in the difference profile at 2$\theta$ values corresponding to the (102) and (103) planes (Fig. 2e). The refinement was repeated by incorporating March function parameters to account for preferred orientation along these directions. The resultant fit was found to be satisfactory (Fig. 2b), and the difference profile (Fig. 2c) was a smooth function. The preferred orientation parameters are given in Table 1.

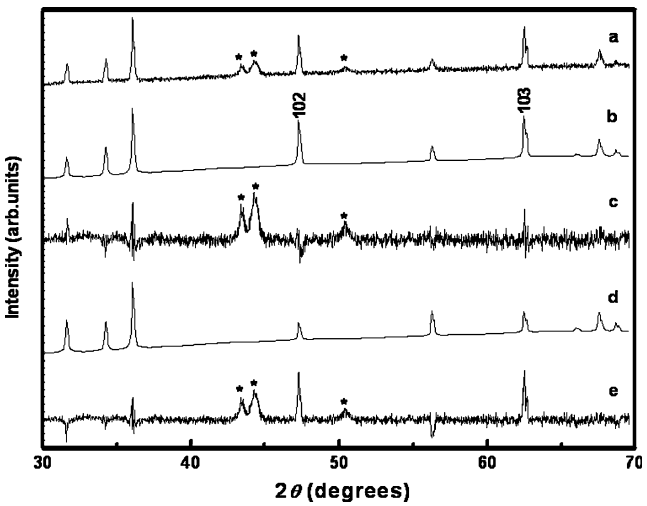


**Fig. 2** **a** XRD profile of a ZnO coating obtained from 40% ($v/v$) isopropanol bath compared with **b** the calculated XRD profile incorporating the effect of orientation and **c** the corresponding difference profile. **d**, **e** The calculated XRD profile and difference profile, respectively, obtained before the incorporation of orientation effects. Features marked by the *asterisk* are due to the stainless steel substrate and were excluded for the Rietveld fits

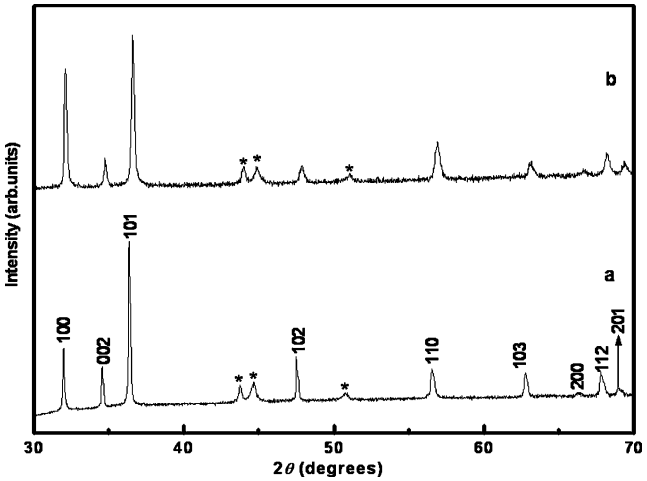


**Fig. 3** XRD profile of ZnO coatings obtained from **a** 50% (*v*/*v*) and **b** 60% (*v*/*v*) isopropanol baths. Features marked by the *asterisk* are due to the stainless steel substrate

The ZnO coatings obtained at still higher IPA concentrations (~50%, *v*/*v*) yield unoriented coatings with no reflection appearing with anomalous intensity (Fig. 3a). At 60% (*v*/*v*) IPA concentration, anomalous growth in the intensity of the peak due to the (100) plane was observed (Fig. 3b). This anomalous growth is evident in the residual intensities observed in the difference profile obtained at the end of the Rietveld refinement procedure (Supporting Information SI 2). Incorporation of a bi-axial orientation in the [100] and [110] directions led to a smooth difference profile (SI 2; Table 1).

The scanning electron microscope (SEM) image of the ZnO coating obtained from an aqueous bath reveals the cross section of hexagonal columnar crystallites (Fig. 4a). The long axis of the hexagonal column, also the *c*-crystallographic axis, is normal to the substrate accounting for the observed [001] orientation (XRD in Fig. 1a).

Crystal growth during electrochemical deposition takes place under the potential gradient in the double layer presumably by the layer-by-layer accretion of atoms from solution. The (001) plane of ZnO is polar and crystal growth takes place by the accretion of alternative layers of $Zn^{2+}$ and $O^{2-}$ ions. Generally, growth normal to the polar planes is very high, causing them to disappear. But within the wurtzite structure, the polarity of the (001) plane is very small given the small distance $d_{12}$ (see [28]) between the successive $Zn^{2+}$ and $O^{2-}$ layers. Consequently, growth rate along [010] is higher than that along [001] [29]. Further, within the wurtzite structure, the (010), (100), and (110) planes are crystallographically equivalent [30], accounting for their nearly equal incidence as faces of the hexagonal columns (Fig. 4b). Similar morphologies are widely reported in earlier papers [11–18, 20, 22, 23].

The (102)/(103) orientation of the coatings is obtained when the crystallites are tilted to bring the [102]/[103] directions normal to the substrate surface (Fig. 5). This requires a rotation of the hexagonal columns about the *b*-axis. The SEM images clearly show the tilt of the faces of the hexagonal columns with respect to the substrate surface. By the same argument, loss of orientation of coatings obtained at 50% (*v*/*v*) IPA arises due to the random tilt of crystallites with respect to the normal to the surface. The SEM image of the unoriented coating shows clusters of well-facetted crystallites, which appear to be products of gregarious secondary crystallization (Fig. 6a). Even in regions where outgrowths due to secondary crystallization are not there, the crystallites grow with their vertices rather than their faces protruding out of the substrate surface. The biaxial orientation along [100] and [110] observed in coatings deposited at 60% (*v*/*v*) IPA orientation is expected if the hexagonal columns are rotated about the *b*-axis by 90°. However, degree of orientation is very small (Table 1; $G_2$=~0.7), and the SEM image of the coating (Fig. 6b) shows a few scattered rectangular faces of the supine hexagonal columns.

The question arises as to why the direction of orientation changes with increasing IPA content. One possible reason

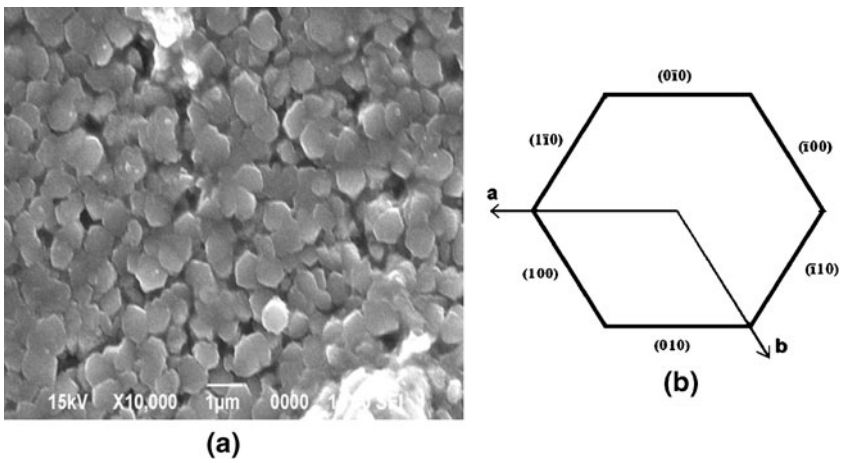


**Fig. 4** **a** Scanning electron micrograph of end faces of hexagonal columns of ZnO deposited from an aqueous bath. **b** A schematic showing the crystallographic planes forming the six faces of the ZnO columns

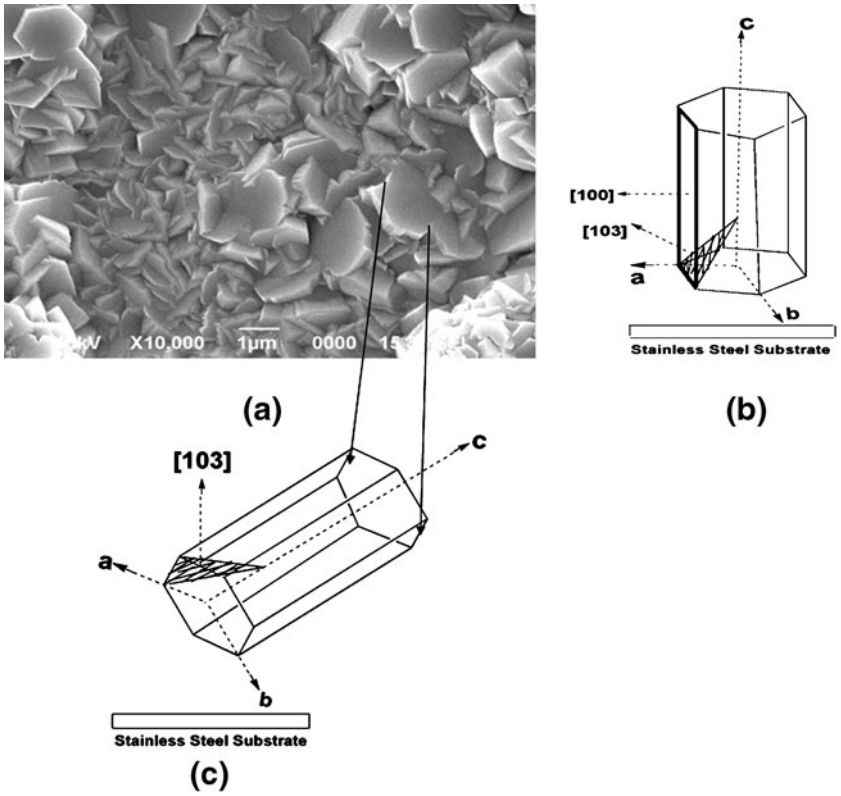


**Fig. 5** **a** Scanning electron micrograph of a ZnO coating oriented along [103] obtained from 40% (*v*/*v*) IPA bath. Schematics **b** and **c** represent hexagonal columns of ZnO oriented along [001] and [103] directions, respectively

could be the change in the dielectric constant of the bath. A polar crystal face would be stabilized in a bath with a high dielectric constant and specially so when it is polarized by an external field as in an electrochemical cell. These forces are considerably reduced when the dielectric constant of the solvent is decreased, thereby enabling the accumulation of crystal faces of lower polarity. A convenient way of changing the dielectric constant of the bath in a continuous manner is by making a mixture of two miscible liquids having different dipole moments. The dielectric constant of the mixed water–IPA solvent changes from 66.62 to 28.9 as the IPA concentration is raised from 0% to 60% (*v*/*v*) at the deposition temperature (60 °C) [31].

Many parameters affect the outcome of an electrodeposition process. These include the interfacial pH, diffusion controlled mass transport as well as mechanical transport in stirred solutions, equilibria, and reaction kinetics of chemical and electrochemical processes. Both thermodynamic and kinetic factors are involved, making the theoretical modeling of electrodeposition a complex process. Mandin and coworkers [32, 33] have extensively modeled the electrodeposition process to numerically evaluate the interfacial pH and reactant concentrations and applied their model to understanding the deposition of ZnO. These models [32] predict speciation, porosity, and morphological microstructure, but not the crystal structure and

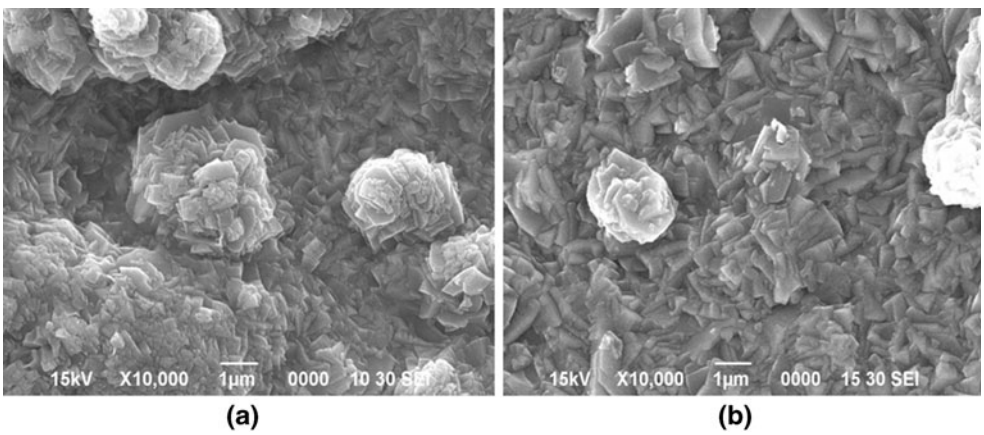


**Fig. 6** Scanning electron micrograph of **a** an unoriented ZnO coating obtained from 50% (*v*/*v*) IPA bath and **b** a ZnO coating with a bi-axial orientation obtained from 60% (*v*/*v*) IPA bath

film texture. Developing a complete theoretical model to predict film texture and relate it to the dielectric constant of the solvent is outside the scope of this paper. Nevertheless, this study generates the possibility of exploring a variety of mixed baths to tailor-oriented crystallization of different semiconducting oxides.

## Conclusion

In conclusion, the orientation of an electrodeposited ZnO coating could be switched from the commonly observed [001] to other directions by varying the solvent composition. This is an illustration of solution mediated control over oriented crystallization in contrast with the better known substrate-controlled orientation by epitaxy. Solution-mediated crystallization provides a way of growing oriented coatings on polycrystalline substrates for a variety of possible applications.

**Acknowledgments** The authors thank the University Grants Commission, Government of India (GOI) for financial support. PVK is a recipient of the Ramanna Fellowship of the Department of Science and Technology, GOI.

## References

1. Hartnagel HL, Dawar AL, Jain AK, Jagadish C (1995) Semiconducting transparent thin films. Institute of Physics, Bristol
2. Park WI, Yi GC (2004) Adv Mater 16:87
3. Hosono E, Fujihara S, Kimuna T (2004) Electrochem Solid-State Lett 7:C49
4. Jacobs H, Mokwa W, Kohi D, Heiland G (1985) Surf Sci 160:217
5. Pern AS (1994) Am Ceram Soc Bull 73:139
6. Stolt L, Hedstrom J, Ruckh M, Kessler J, Velthaus KO, Schock HW (1993) Appl Phys Lett 62:597
7. Weans WW, Yamada A, Konagai M, Takahashi K (1994) J Appl Phys 33:283
8. Sang B, Konagai M (1996) J Appl Phys 35:602
9. Bae SY, Seo HW, Park J (2004) J Phy Chem B 108:5206
10. Izaki M, Omi T (1996) J Electrochem Soc 143:L53
11. Izaki M, Omi T (1996) Appl Phys Lett 68:2439
12. Izaki M, Omi T (1997) J Electrochem Soc 144:1949
13. Peulon S, Lincot D (1996) Adv Mater 8:166
14. Peulon S, Lincot D (1998) J Electrochem Soc 145:864
15. Pauporte T, Lincot D (1999) Appl Phys Lett 75:3817
16. Pauporte T, Lincot D (2000) Electrochim Acta 45:3345
17. Canava B, Lincot D (2000) J Appl Electrochem 30:711
18. Pauporte T, Lincot D (2001) J Electrochem Soc 148:C310
19. Pauporte T, Lincot D (2001) J Electroanal Chem 517:54
20. Pauporte T, Cortes R, Froment M, Beaumont B, Lincot D (2002) Chem Mater 14:4702
21. Goux A, Pauporte T, Chivot J, Lincot D (2005) Electrochim Acta 50:2239
22. Liu R, Vertegel AA, Bohannan EW, Sorenson TA, Switzer JA (2001) Chem Mater 13:508
23. Limmer SJ, Kulp EA, Switzer JA (2006) Langmuir 22:10535
24. Jayakrishnan R, Hodes G (2003) Thin Solid Films 440:19
25. Lin KF, Cheng HM, Hsu HC, Lin LJ, Hsieh WF (2005) Chem Phys Lett 409:208
26. Prasad BE, Kamath PV, Upadhya S (2008) J Am Ceram Soc 91:3870
27. Joseph S, Kamath PV (2007) J Electrochem Soc 154:E102
28. Meyer B, Marx D (2003) Phys Rev B 67:035403
29. Li WJ, Shi EW, Zhong WZ, Yin ZW (1999) J Cryst Grow 203:186
30. Wang ZL (2004) J Phys Condens Matter 16:R829
31. Akerlof G (1932) J Am Chem Soc 54:4125
32. Mandin Ph, Cense JM, Picard G, Lincot D (2006) Electrochim Acta 52:1296
33. Mandin Ph, Cense JM, Fabian C, Lincot D (2007) Comp Chem Eng 31:980